(Received 17 November 2023, Accepted 26 January 2024, Scheduled 26 February 2024)

A Fast Coupled Iterative Approach for Computing 3D Composite Scattering from Dielectric Rough Surfaces and Target

Juan Zhao*

School of Mathematics and Computer Science, Yichun University, Yichun 336000, Jiangxi, China

ABSTRACT: This paper proposes a fast coupled iterative algorithm for calculating the complex three-dimensional scattering of rough dielectric surfaces and conductive targets. The algorithm is designed for practical composite electromagnetic scattering models and establishes a coupled iterative integral equation system for the rough surface and target. Iterative calculations are performed until the specified accuracy is achieved. To improve computational speed, Physics Based Two Grid-Sparse Matrix Canonical Grid (PB-SM) acceleration algorithm and a hybrid domain basis function based on quadratic surface modeling are applied using the fast Method of Moments (MoM) for fast computation. The effectiveness of the fast coupled iterative algorithm is verified by comparing the results with those of high-precision MoM calculations. During the calculation process, error iteration curves are plotted to show that the error can be reduced to 10^{-6} after 10 iterations, and the convergence rate meets the requirements of practical calculations. Based on the algorithm proposed in this paper, several examples are calculated, and the scattering variation of targets in different environments is mainly studied, and suggestions are given to improve the accuracy of target detection and identification in complex environments. The results of the study have some significance for ultra-low altitude target detection, precision strike, stealth and anti-stealth.

1. INTRODUCTION

The scattering field is the result of the interaction between electromagnetic waves and irradiated objects. The scattered echoes from the object usually contain information about the geometric shape and electromagnetic parameters of the irradiated object, providing important information for target recognition [1–4] and feature extraction [5–9].

Modern warfare is a high-tech war with five dimensions: land, sea, air, sky, and electromagnetic, in which the electromagnetic scattering characteristics [10–16] of military targets and complex natural environments are important components of integrated sensory information on the battlefield. For example, when airborne or satellite radar detects and alerts military targets (such as aircraft and missiles) in the actual battlefield environment, its echo signal inevitably contains useless clutter signals reflected back from the natural environment, which will reduce the accuracy of target identification and increase the probability of false alarms. How to eliminate clutter interference in complex natural environment, establish one-to-one correspondence between radar characteristic signals and measured targets, improve early warning judgment of military signals, military target detection, especially detection and remote sensing of actual ground background (bare soil, desert, etc.) and military targets (such as aircraft, missiles, etc.), has long been one of the most important research topics in the field of radar. Therefore, the study of the interaction mechanism and the theoretical model of composite scattering of electromagnetic wave detection signal with the target and the surface of the natural environment is the theoretical basis and prerequisite for reconnaissance, early warning, detection, tracking, identification, guidance and interception of military targets in the actual battlefield environment. The research results of theoretical calculation, target feature extraction and identification will provide important technical support for the precision guidance, simulation, stealth and anti-stealth technologies of our new weapon systems and the whole process of combat.

2. LITERATURE ANALYSIS

The study of target and environmental electromagnetic scattering characteristics is a very important and widely used topic in the field of remote sensing and monitoring. In recent years, with the rapid development of radar remote sensing and target detection technology, the study of target and environmental electromagnetic scattering characteristics [17–24] has received more and more extensive attention from scholars.

Paper [25] comprehensively reviewed and analyzed the basic principles, implementation methods, advantages and disadvantages, and application in practical problems of the large-scale parallel multi-level fast multipole algorithm. This algorithm achieved parallel computing and speedup by decomposing the computation domain into multiple subdomains and performing fast multipole computation in each subdomain. The algorithm combined multi-level fast Fourier transforms (FFT) with the multi-level fast multipole algorithm by decomposing the computation domain into multiple subdomains and performing FFT computation in each subdomain to reduce the computational burden and improve computational efficiency. Addition-

* Corresponding author: Juan Zhao (ncxjj0119@126.com).

ally, the algorithm used parallel computing techniques to allocate computational tasks to multiple processors or computers to achieve faster computational speed. Paper [25] also discussed the parallel performance and computational efficiency of the algorithm and explored how to further improve computational efficiency and accuracy by optimizing algorithm parameters and adjusting parallel strategies.

The node-based DG-PSTD (discontinuous Galerkin-pseudospectral time domain) algorithm proposed in [26] was an effective method for solving three-dimensional large-scale Maxwell's equations. This algorithm combined the advantages of DG and PSTD, and provided stable coupling for multiple domains with unstructured hexagons. In addition, this algorithm had low storage and expandability, and could flexibly handle complex medium modeling. Finally, [26] further proved and demonstrated the efficiency and capability of the proposed high-order solver. The DG-PSTD method proposed in [26] was suitable for dealing with large-scale electromagnetic field problems and had high computational efficiency and accuracy. It had great development prospects in electromagnetic wave propagation, antenna radiation, and electromagnetic compatibility, and could help people better understand the characteristics and behavior of electromagnetic fields.

A new hybrid analysis numerical iterative algorithm that combines Kirchhoff approximation (KA) and Method of Moments (MoM) was discussed in [27] that could effectively reduce the required memory and CPU time for the iterative calculation of the scattering field on the rough surface and the current on the target surface, which reduces the memory and CPU time required for the calculation. In addition, the effectiveness and convergence performance of this algorithm have also been discussed. Finally, through Monte Carlo simulation of random rough surfaces, numerical simulations of bistatic scattering of targets of different shapes on Gaussian rough surfaces were performed, and the relationship between bistatic scattering patterns and surface dielectric properties and target geometry was discussed.

Paper [28] generated the rough surface based on the weighted tangent function and spectrum method to simulate the composite rough surface at the actual land-sea interface and applied a more accurate second-order small slope approximation (SSA-II) to calculate the electromagnetic scattering of the model. The Doppler spectra of this composite rough surface and the sea surface are compared, and it is found that the scattering coefficients of the land-sea composite rough surface are smaller than those of the sea surface under certain polarization modes.

In [29], the time-domain shooting and bouncing rays (TDSBR) method was proposed to study the composite electromagnetic scattering characteristics of the target-ocean, and the inverse synthetic aperture radar (ISAR) imaging equation was derived to obtain the ISAR image of the composite target against the ocean background by further processing the scattered echo data. Meanwhile, to improve the efficiency of the algorithm, Gaussian pulses were used instead of Linear frequency modulation (LFM), and matched filters were improved to achieve pulse compression under modulating Gaussian pulse excitations. Finally, the effectiveness of the TDSBR algorithm was verified by calculating several examples. A hybrid method of extended propagation-inside-layer expansion (EPILE) combined with generalized forward-backward method (GFBM) was proposed in [30], which mainly studied the electromagnetic scattering characteristics of movable/rotatable ship targets in the ocean and analyzed the multiple scattering characteristics under different parameters by several example calculations. Paper [31] mainly studied the composite electromagnetic scattering from a one-dimensional dielectric rough surface with a coated target, and proposed and derived a hybrid algorithm based on finite element method (FEM) and boundary integral method (BIM) in detail. The algorithm applied FEM to calculate the electromagnetic field inside the coated target and BIM to calculate the composite electromagnetic field with the target-rough surface, respectively. To ensure the accuracy of modeling, the boundary conditions were carefully analyzed, and the effectiveness of FEM-BIM was verified by the MoM algorithm. Finally, [31] studied the two-dimensional scattering characteristics under different conditions by several examples, while the actual target and rough surface are three-dimensional, if He and Zhang's research results can be extended to the study of three-dimensional scattering, then the practicality will be greatly enhanced.

This article combines the PB-SM method, mutual coupling iteration method, and fast MoM method to analyze the composite scattering of rough surface and target in general three-dimensional scattering problems. The rough surfaces are usually characterized by Gaussian function [32], and the target often has conductor properties. PB-SM is used to accelerate the calculation of rough surface scattering; fast MoM is used to accelerate the calculation of target scattering; and their interaction is updated through iterative processes to achieve excitation terms. It is found that after 10 iterations, the error can be reduced to 10^{-6}, and the convergence speed meets the requirements of practical calculations. Finally, several examples of target-environment interactions were studied. The study found that using a reasonable shape design can greatly suppress the coupling scattering effect between the aircraft and the environment, thereby achieving the goal of reducing the rear radar cross-section (RCS) of the aircraft at certain angles (such as the direction of incoming cruise missiles) and improving the aircraft's survivability.

3. GAUSSIAN ROUGH SURFACE MODELING

The random roughness of the surface in nature can be regarded as a random distribution of features with specific probabilities. In numerical calculations, it is necessary to use random roughness with specific spectral functions to simulate actual surfaces and sea surfaces. The electromagnetic scattering characteristics of rough surfaces with different characteristics are significantly different. Therefore, the generation of rough surfaces is an important foundation for ensuring the accuracy of electromagnetic scattering characteristics calculations.

In this paper, a combination of Gaussian spectrum function and Monte Carlo method is used to generate Gaussian-type rough surfaces to simulate actual ground surfaces in order to re-

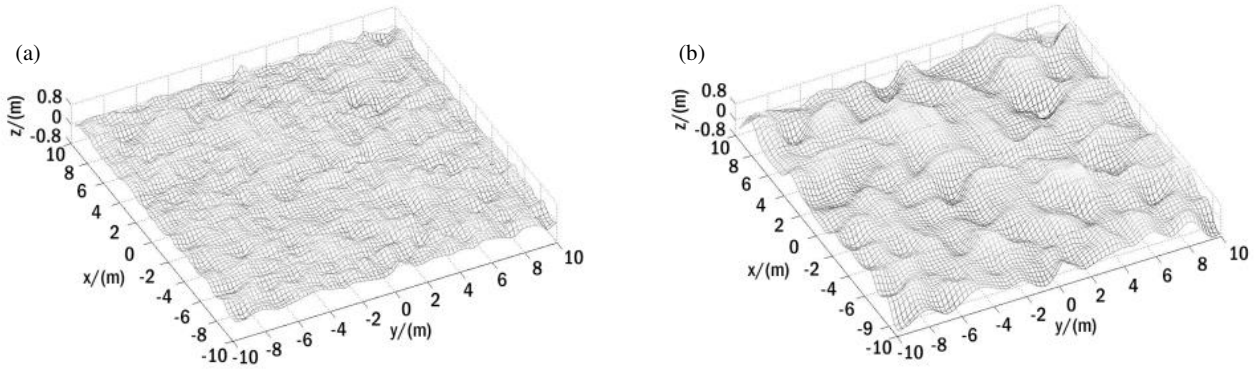

FIGURE 1. Two-dimensional Gaussian rough surface: (a) $h = 0.1\,\text{m}$, $l_x = l_y = 0.5\,\text{m}$ and (b) $h = 0.3\,\text{m}$, $l_x = l_y = 1.0\,\text{m}$.

produce the actual ground state as much as possible. The height profile function $f(x, y)$ of the rough surface is expressed by the fast Fourier transform as [32]:

$$f(x,y) = \frac{1}{L_x L_y} \sum_{m=-\infty}^{\infty} \sum_{n=-\infty}^{\infty} b_{mn} \exp\left(\frac{j2\pi mx}{L_x}\right) \exp\left(\frac{j2\pi ny}{L_y}\right) \quad (1)$$

where m, n are the two subscripts of the summation symbol, which is traversal over all discrete points. (m, n) can represent a discrete point position. b_{mn} is the coefficient, and the expression is:

$$b_{mn} = 2\pi\sqrt{L_x L_y W(K_{xm}, K_{yn})} \cdot \begin{cases} \frac{N(0,1)+jN(0,1)}{\sqrt{2}} & m \neq 0, N_x/2, n \neq 0, N_y/2 \\ N(0,1) & m = 0, N_x/2 \text{ or } n = 0, N_y/2 \end{cases} \quad (2)$$

$W(K_x, K_y)$ is the Gaussian spectral function of the two-dimensional rough surface, representing the power spectral density of the two-dimensional rough surface:

$$W(K_x, K_y) = \frac{l_x l_y h^2}{4\pi} \exp\left(-\frac{K_x^2 l_x^2}{4} - \frac{K_y^2 l_y^2}{4}\right) \quad (3)$$

where x and y represent the two directions of the axes; l_x, l_y are the correlation lengths in the x and y directions, respectively; h is the root mean square height; $N(0, 1)$ is a sampling point of a sequence of random numbers with mean zero and variance normally distributed; K_{xm} and K_{yn} are the discrete points of the spatial frequencies in the x and y directions, respectively; L_x and L_y are the contour lengths of the rough surface in the x and y directions, respectively, and:

$$K_{xm} = \frac{2\pi m}{L_x} \quad K_{yn} = \frac{2\pi n}{L_y} \quad (4)$$

In order to ensure that the height $f(x, y)$ of the rough surface is real-valued, the coefficient b_{mn} must satisfy the conjugate symmetry with respect to the origin, that is, any point reflection with respect to the origin is its conjugate symmetric point. Only in this way can we ensure that the contour function $f(x, y)$ obtained by inverse Fourier transform is real and consistent with the actual situation, so:

$$b(m,n) = b^*(-m,-n) \quad b(m,-n) = b^*(-m,n) \quad (5)$$

The first order partial derivatives $f'_x(x_m, x_n)$, $f'_y(x_m, x_n)$ of $f(x, y)$ with respect to x and y can be solved from Eq. (1):

$$f'_x(x_m, y_n) = \frac{1}{L_x L_y} \cdot \sum_{p=-\frac{N_x}{2}+1}^{\frac{N_x}{2}} \sum_{q=-\frac{N_y}{2}+1}^{\frac{N_y}{2}} b_{mn} \left(\frac{j2\pi p}{L_x}\right) \exp\left(\frac{j2\pi px_m}{L_x}\right) \exp\left(\frac{j2\pi qy_n}{L_y}\right) \quad (6)$$

$$f'_y(x_m, y_n) = \frac{1}{L_x L_y} \cdot \sum_{p=-\frac{N_x}{2}+1}^{\frac{N_x}{2}} \sum_{q=-\frac{N_y}{2}+1}^{\frac{N_y}{2}} b_{mn} \left(\frac{j2\pi q}{L_y}\right) \exp\left(\frac{j2\pi px_m}{L_x}\right) \exp\left(\frac{j2\pi qy_n}{L_y}\right) \quad (7)$$

$f(x, y), f'_x(x_m, x_n), f'_y(x_m, x_n)$ are all in the form of two-dimensional Discrete Fourier Transform (DFT), and they can all be computed quickly with the two-dimensional FFT algorithm [32].

According to the above method, two-dimensional Gaussian rough surfaces with different parameters (root mean square height, correlation length) can be simulated and generated, as shown in Fig. 1. The specific generation process can be referred to [33] and will not be further explained here.

4. FAST COUPLED ITERATIVE APPROACH MODEL

In the calculation of composite scattering between a rough surface and a target in two dimensions, the large amount of data in matrix equations and the low efficiency of direct calculation make the study of fast algorithms an important topic. Previous methods have modeled the target and surface as a whole as well as solved them, and since numerical algorithms have to generate matrix equations, this leads to an excessive amount of matrix data and cannot be solved quickly. To solve this problem,

this paper proposes a fast coupled iterative numerical algorithm, using different acceleration algorithms to calculate the surface electric and magnetic currents of the rough surface and the target respectively, so as to calculate the mutual scattering field, and so on iteratively, setting the convergence conditions until the convergence requirements are met, that is, the fast coupled iterative numerical algorithm for the two-dimensional medium rough surface and its three-dimensional conductor target above. This process is explained in detail below.

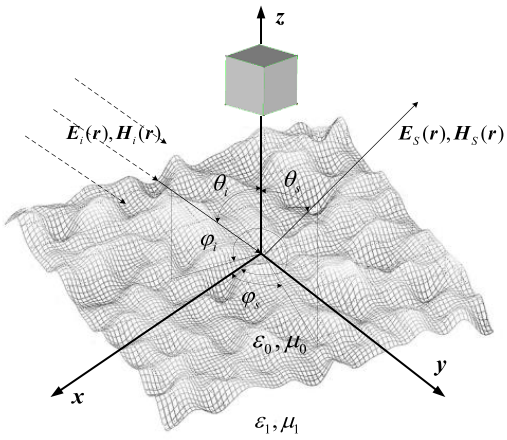

FIGURE 2. Composite scattering diagram.

4.1. Fast Coupled Iterative Approach Model

The composite scattering diagram of the rough surface and the target is shown in Fig. 2. When the field point $\mathbf{r}$ is close to the rough surface S_r, the surface integral equations are:

$$\mathbf{n}\cdot(\mathbf{E}_{inc}(\mathbf{r})+\mathbf{E}_o^s(\mathbf{r}))=\frac{\mathbf{I}_n(\mathbf{r})}{2}-\mathbf{n}\cdot\left\{\int_{S_r}j\omega\mu_0\mathbf{J}_s(\mathbf{r}')\,g_0(\mathbf{r},\mathbf{r}')\,ds'+P\int_{S_r}[\mathbf{M}_s(\mathbf{r}')\times\nabla' g_0(\mathbf{r},\mathbf{r}')+\nabla' g_0(\mathbf{r},\mathbf{r}')\cdot\mathbf{I}_n(\mathbf{r}')]\,ds'\right\} \tag{8}$$

$$\mathbf{n}\times(\mathbf{H}_{inc}(\mathbf{r})+\mathbf{H}_o^s(\mathbf{r}))=\frac{\mathbf{J}_s(\mathbf{r})}{2}+\mathbf{n}\times\left\{\int_{S_r}j\omega\varepsilon_0\mathbf{M}_s(\mathbf{r}')\,g_0(\mathbf{r},\mathbf{r}')\,ds'-P\int_{S_r}[\nabla' g_0(\mathbf{r},\mathbf{r}')\cdot\mathbf{F}_n(\mathbf{r}')+\int_{S_r}\mathbf{J}_s(\mathbf{r}')\times\nabla' g_0(\mathbf{r},\mathbf{r}')\right]ds'\right\} \tag{9}$$

$$0=-\frac{\mathbf{n}\times\mathbf{E}(\mathbf{r})}{2}-\mathbf{n}\times\left\{\int_{S_r}j\omega\mu_1\mathbf{n}'\times\mathbf{H}(\mathbf{r}')\,g_1(\mathbf{r},\mathbf{r}')\,ds'+P\int_{S_r}[(\mathbf{n}'\times\mathbf{E}(\mathbf{r}'))\times\nabla' g_1(\mathbf{r},\mathbf{r}')+\nabla' g_1(\mathbf{r},\mathbf{r}')\frac{\varepsilon_0}{\varepsilon_1}\mathbf{n}'\cdot\mathbf{E}(\mathbf{r}')\right]ds'\right\} \tag{10}$$

$$0=-\frac{\mathbf{n}\cdot\mathbf{H}(\mathbf{r})}{2}+\mathbf{n}\cdot\left\{\int_{S_r}j\omega\varepsilon_1\mathbf{n}'\times\mathbf{E}(\mathbf{r}')\,g_1(\mathbf{r},\mathbf{r}')\,ds'-P\int_{S_r}\left[\nabla' g_1(\mathbf{r},\mathbf{r}')\frac{\mu_0}{\mu_1}\mathbf{n}'\cdot\mathbf{H}(\mathbf{r}')+(\mathbf{n}'\times\mathbf{H}(\mathbf{r}'))\times\nabla' g_1(\mathbf{r},\mathbf{r}')\right]ds'\right\} \tag{11}$$

where S_r represents the rough surface; $\mathbf{H}_{inc}(\mathbf{r})$ and $\mathbf{E}_{inc}(\mathbf{r})$ are the incident electromagnetic fields; $P\int$ represents the integral without singular points; and the medium parameters in the space below the rough surface are (ε_1,μ_1). The medium above the rough surface is free space with parameters (ε_0,μ_0), and g_0 and g_1 are the Green's functions in free space and rough surface medium. $\mathbf{r}$ represents the field point; $\mathbf{r}'$ represents the source point; ω is the angle frequency of the incident wave.

$\mathbf{M}_s=\mathbf{n}\times\mathbf{E}$ represents the electromagnetic induction current on a rough surface; $\mathbf{J}_s=\mathbf{n}\times\mathbf{H}$ represents the induced current on a rough surface; and there are $\mathbf{I}_n=\mathbf{n}\cdot\mathbf{E}$ and $\mathbf{F}_n=\mathbf{n}\cdot\mathbf{H}$.

$\mathbf{E}_o^s(\mathbf{r})$ and $\mathbf{H}_o^s(\mathbf{r})$ are the scattered fields from the target,

$$\mathbf{H}_o^s(\mathbf{r})=-\int_{S_o}\mathbf{J}_0(\mathbf{r}')\times\nabla' g_0(\mathbf{r},\mathbf{r}')ds' \tag{12}$$

$$\mathbf{E}_o^s(\mathbf{r})=-\frac{i}{\omega\varepsilon_o}\nabla\times\int_{S_o}\mathbf{J}_o(\mathbf{r}')\times\nabla' g_0(\mathbf{r},\mathbf{r}')ds' \tag{13}$$

In the above equation, $\mathbf{J}_o(\mathbf{r})$ is the target surface current. When the field point $\mathbf{r}$ is close to the rough surface, the integral equation of the target is:

$$(\mathbf{E}_{inc}(\mathbf{r})+\mathbf{E}_r^s(\mathbf{r}))|_{\tan}=i\omega\mu_0 P\int_{S_o}\left[\mathbf{J}_o(\mathbf{r}')+\frac{1}{k_0^2}\nabla(\nabla'\cdot\mathbf{J}_o(\mathbf{r}'))\right]g_0(\mathbf{r},\mathbf{r}')ds'\Big|_{\tan} \tag{14}$$

where

$$\mathbf{E}_r^s(\mathbf{r})=-\int_{S_r}[(-i\omega\mu_0)\mathbf{J}_s(\mathbf{r}')g_o+\mathbf{M}_s(\mathbf{r}')\times\nabla' g_o+\nabla' g_o\mathbf{I}_n(\mathbf{r}')]\,ds' \tag{15}$$

Eqs. (12)–(15) are the set of composite scattering integral equations for the rough surface of the medium and the conductor target above.

If the above system of equations is calculated directly, the computation is very large and will consume huge memory and time, which is unacceptable in practice. For this reason, a mutually coupled iterative approach is used to speed up the computation process. The iterative process of the nth step is listed below:

$$\mathbf{n}\cdot\left(\mathbf{E}_{inc}(\mathbf{r})+\mathbf{E}_o^{s,(n-1)}(\mathbf{r})\right)=\frac{\mathbf{I}_n^{(n)}(\mathbf{r})}{2}-\mathbf{n}\cdot\left\{\int_{S_r}j\omega\mu_0\mathbf{J}_s^{(n)}(\mathbf{r}')\,g_0(\mathbf{r},\mathbf{r}')\,ds'+P\int_{S_r}\left[\mathbf{M}_s^{(n)}(\mathbf{r}')\times\nabla' g_0(\mathbf{r},\mathbf{r}')+\nabla' g_0(\mathbf{r},\mathbf{r}')\,\mathbf{I}_n^{(n)}(\mathbf{r}')\right]ds'\right\} \tag{16}$$

$$\mathbf{E}_r^s(\mathbf{r}) = -\int_{S_r} [(-i\omega\mu_0)\mathbf{J}_s(\mathbf{r}')g_o + \mathbf{M}_s(\mathbf{r}') \times\nabla' g_o + \nabla' g_o \mathbf{I}_n(\mathbf{r}')]\, ds' \tag{17}$$

$$(\mathbf{E}_{inc}(\mathbf{r}) + \mathbf{E}_r^{s,(n)}(\mathbf{r}))\Big|_{\tan} = i\omega\mu_0 P \int_{S_o} \left[\mathbf{J}_o^{(n)}(\mathbf{r}') + \frac{1}{k_0^2}\nabla(\nabla'\cdot\mathbf{J}_o^{(n)}(\mathbf{r}'))\right] g_0(\mathbf{r},\mathbf{r}')ds'\Big|_{\tan} \tag{18}$$

$$\mathbf{H}_o^{s,(n)}(\mathbf{r}) = -\int_{S_o} \mathbf{J}_o^{(n)}(\mathbf{r}') \times \nabla' g_0(\mathbf{r},\mathbf{r}')ds' \tag{19}$$

The initial values of the iterations are:

$$\mathbf{J}_o^{(0)} = 0,\ \ \mathbf{J}_s^{(0)} = 0,\ \ \mathbf{H}_o^{s,(0)} = 0,\ \ \mathbf{E}_r^{s,(0)} = 0 \tag{20}$$

First, substitute the initial value into Eq. (16) to obtain $\mathbf{J}_s^{(1)}$. Then, update $\mathbf{E}_r^{s,(1)}$ by substituting $\mathbf{J}_s^{(1)}$ into Eq. (17). Next, update $\mathbf{J}_o^{(1)}$ by substituting the updated $\mathbf{E}_r^{s,(1)}$ into Eq. (18). Finally, update $\mathbf{H}_o^{s,(1)}$ based on the updated $\mathbf{J}_o^{(1)}$ using Eq. (19). After one iteration, the updated values of $\mathbf{J}_s^{(1)}$, $\mathbf{J}_o^{(1)}$, $\mathbf{H}_o^{s,(1)}$, and $\mathbf{E}_r^{s,(1)}$ are obtained. The process is repeated from the beginning for the next iteration. The iterative process can be referred to as shown in Fig. 3.

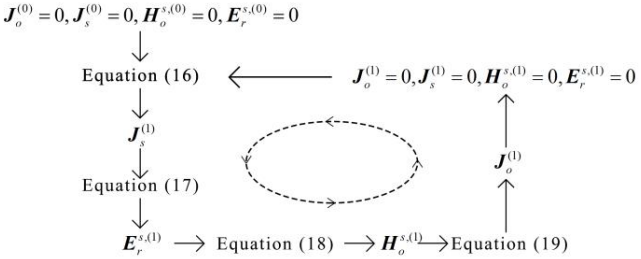

FIGURE 3. Iterative diagram.

The iterative calculation is repeated until the accuracy meets the requirement, and the iterative convergence error of the nth step is defined as [34]:

$$\tau(n) = \left|\frac{\mathbf{Z}_o(\mathbf{J}_o^{(n)} - \mathbf{J}_o^{(n-1)})}{\mathbf{Z}_o\mathbf{J}_o^{(n)}}\right| \tag{21}$$

The iterative algorithm has a clear physical meaning: after the first iteration, $\mathbf{J}_s^{(n)}$ denotes the current distribution of the rough surface when only the incident wave is considered; $\mathbf{J}_o^{(n)}$ denotes the current distribution of the target surface when the first scattering of the incident wave and the rough surface to the target is considered; $\mathbf{H}_o^{s,(n)}$ denotes the first scattering of the target to the rough surface; $\mathbf{E}_r^{s,(n)}$ denotes the first scattering of the rough surface to the target; the number of iterations n denotes the nth order scattering.

In the calculation, if the scattering from the rough surface and target is solved directly, there will be a large number of unknown quantities, which leads to long computation time and low efficiency. To solve this problem, accelerated algorithms are used in the calculation to calculate the scattering from the rough surface and the target separately to improve the computational efficiency.

The process is: applying the PB-SM accelerated algorithm to calculate the scattering from the rough surface and applying the fast MoM algorithm to calculate the scattering from the target. These two algorithms are introduced in detail next.

4.2. PB-SM Fast Algorithm

Firstly, the vector surface area integration equation of the medium rough surface is expanded into six scalar surface area integration equations in each direction, and a dense interpolation is performed to obtain the following expression. The specific processing process can be found in [35] and is not repeated here for space saving.

$$\sum_{n=1}^{N}\sum_{q=1}^{6} Z_{mn}^{pq} I_n^{(q)} = I_m^{(p)inc} \tag{22}$$

where N is the number of discrete nodes on the rough surface, Z_{mn}^{pq} the impedance matrix, and $I_n^{(q)}$ the unknown quantity to be solved.

Then the relevant distance r_d is defined, and the field point on the rough surface is considered as near field when the distance R between the field point and the source point is less than r_d, and is considered as far field when R is greater than r_d. The matrix equation can then be expressed as a near-field strong correlation matrix $\mathbf{Z}^{(s)}$ and a far-field weak correlation matrix $\mathbf{Z}^{(w)}$ in the form of:

$$\left(\mathbf{Z}^{(s)} + \mathbf{Z}^{(FS)}\right)\mathbf{X}^{(n+1)} = \mathbf{b} - \mathbf{Z}^{(w)}\mathbf{X}^{(n)} \tag{23}$$

The matrix equation is iterated in the form of:

$$\left(\mathbf{Z}^{(s)} + \mathbf{Z}^{(FS)}\right)\mathbf{x}^{(1)} = \mathbf{b}_{inc} \tag{24}$$

$$\left(\mathbf{Z}^{(s)} + \mathbf{Z}^{(FS)}\right)\mathbf{x}^{(n+1)} = \mathbf{b}_{inc}^{(n+1)} \tag{25}$$

When $\sqrt{\left\|\mathbf{b}_{inc}^{(n)}\right\| / \|\mathbf{b}_{inc}\|} \times 100\% < \sigma$, the iteration ends. $\mathbf{Z}^{(FS)}$ and $\mathbf{Z}^{(w)}$ can be expressed as the sum of several Toeplitz matrices, and the FFT can be used to quickly calculate the matrix vector product and speed up the computation. However, this is not enough, and it can be faster on top of that.

Then the rough surface is divided into Single Coarse Grid and Single Dense Grid by two profile densities, whereupon the matrix equation can be decomposed as: matrix of rough surfaces in medium space, the far-field matrix of rough surfaces in free space, and the near-field matrix of rough surfaces in free space.

For matrix of rough surfaces in medium space: As the dielectric space has a large dielectric constant imaginary part, the loss of dielectric space Green's function is large, then it can be considered that if the distance between two points is greater than r_l ($r_l = C/k_2''$, k_2'' is the imaginary part of k_2 in the medium space), and the impedance matrix is equal to 0, so the

impedance matrix of the dielectric rough surface can be approximated as:

$$\mathbf{Z}_{mn}^{pq} = \tilde{\mathbf{Z}}_{mn}^{pq} = \begin{cases} \mathbf{Z}_{mn}^{pq} & r_{mn} \le r_l \\ 0 & r_{mn} \ge r_l \end{cases} \tag{26}$$

r_{mn} is the distance between nodes m and n, so the matrix equation for the rough surface of the medium becomes:

$$\sum_{n=1}^{N_{sdg}} \sum_{q=1}^{6} \tilde{\mathbf{Z}}_{mn}^{pq} I_n^{(q)} = I_m^{(p)inc} \tag{27}$$

where $\mathbf{Z}_{mn}^{pq}$ is a sparse band matrix, and N_{sdg} is the total number of nodes in the single dense grid:

$$N_{sdg} = \left(n_{sdg} \frac{L_x}{\lambda}\right)\left(n_{sdg} \frac{L_y}{\lambda}\right) \tag{28}$$

L_x, L_y are the size of the rough surface, and λ is the wavelength.

For the far-field matrix of rough surfaces in free space: Since the Green's function of the free space far field is slowly varying, the surface electromagnetic field on Single Dense Grid nodes can be averaged in the matrix, applied to the Single Coarse Grid nodes, and then multiplied with the impedance matrix of the sparse profile nodes to obtain:

$$\begin{aligned} &\sum_{l=1}^{n_2^2} \mathbf{Z}_{(m+l)(n+l)}^{pq} I_{n+l}^{(q)} \approx \mathbf{Z}_{m_{mp}n_{mp}}^{pq} \sum_{l=1}^{n_2^2} I_{n+l}^{(q)} \\ &= n_2^2 \mathbf{Z}_{m_{mp}n_{mp}}^{pq} \left(\frac{1}{n_2^2} \sum_{l=1}^{n_2^2} I_{n+l}^{(q)}\right) \end{aligned} \tag{29}$$

For the near-field matrix of rough surfaces in free space: In the near field on the free space rough surface, the rate of change of the Green's function is approximately the same, then the impedance matrix of the free space rough surface can be decomposed into the near field matrix $\mathbf{Z}_{mn}^{pq(s)}$ and far field matrix $\mathbf{Z}_{mn}^{pq(ns)}$ as:

$$\sum_{n=1}^{N_{sdg}} \mathbf{Z}_{mn}^{pq} I_n^{(q)} = \sum_{n=1}^{N_{sdg}} \mathbf{Z}_{mn}^{pq(s)} I_n^{(q)} + \sum_{n=1}^{N_{sdg}} \mathbf{Z}_{mn}^{pq(ns)} I_n^{(q)} \tag{30}$$

Introducing the impedance matrix $\tilde{\mathbf{Z}}_{\tilde{m}\tilde{n}}^{pq}$ of the free space rough surface Single Coarse Grid nodes, the matrix equation of the free space rough surface Single Coarse Grid nodes can be expressed as:

$$\begin{aligned} &\sum_{q=1}^{6} \sum_{n=1}^{N_{sdg}} \mathbf{Z}_{mn}^{pq(s)} I_n^{(q)} + \sum_{q=1}^{6} \left[\sum_{\tilde{n}=1}^{N_{scg}} \tilde{\mathbf{Z}}_{\tilde{m}\tilde{n}}^{pq(ns)} \tilde{I}_{\tilde{n}}^{(q)}\right]_{intp} \\ &= I_m^{(p)inc} \end{aligned} \tag{31}$$

So in this way, the original matrix equations are decomposed into the near-field strongly correlated matrix, planar Toeplitz matrix, and far-field weakly correlated matrix, and then their properties are used in the iterative method to quickly calculate the matrix vector product respectively, which achieves the purpose of accelerating the calculation.

4.3. Fast MoM Algorithm Based on Hybrid Domain Basis Function

In MoM, the current basis function is an important factor affecting the speed and stability of the matrix solution. There are two most commonly used basis functions, one called the full-domain basis and the other called the partitioned basis. The full-domain basis functions are difficult to implement on complex boundaries, but are highly accurate and relatively easy to program, while the fractional-domain basis functions are the opposite. Therefore, it can be considered to combine the advantages of both basis functions and propose a hybrid domain basis function.

In the hybrid domain basis function, the full-domain basis component on the cell boundary is zero, and the current continuity between cells relies on the basis component of each partition to ensure it. In this way, the hybrid domain basis function combines the advantages of good convergence of the full-domain basis component and high numerical stability of the partitioned basis component. Thus, when using mixed-domain basis functions, coarse mesh dissection of the target is possible, and the target can be decomposed into a small number of bilinear surface cells of electrically large size, which greatly reduces the number of unknown quantities.

In principle, the choice of u and v coordinates for bivariate fourth-order quadrilateral can be arbitrary. Assume that the bivariate fourth-order quadrilateral m is adjacent to the bivariate fourth-order quadrilateral n, and compared to the adjacent common edge, there are 16 possible ways for the four edges of element m and the four edges of element n to be adjacent, as shown in Fig. 4. The adjacent ways can be divided into four categories: (a) both normal and tangential directions are in the same direction; (b) the normal direction is opposite, and the tangential direction is in the same direction; (c) both normal and tangential directions are opposite; (d) both normal and tangential directions are in the opposite direction.

During the calculation process, the establishment of local coordinates requires that the tangential current directions of adjacent elements be continuous, as shown in Figs. 5(a) and (b). This requirement adds many difficulties to geometric modeling. However, hybrid domain basis functions can break through these limitations and automatically recognize local coordinates

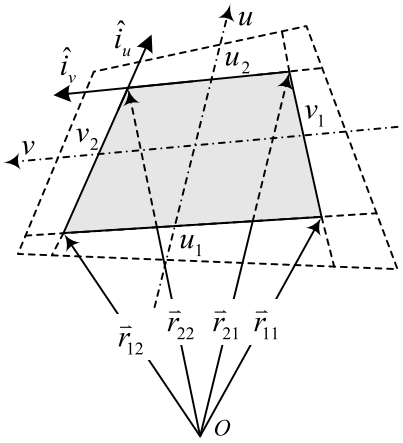

FIGURE 4. Bilinear surface coordinate system.

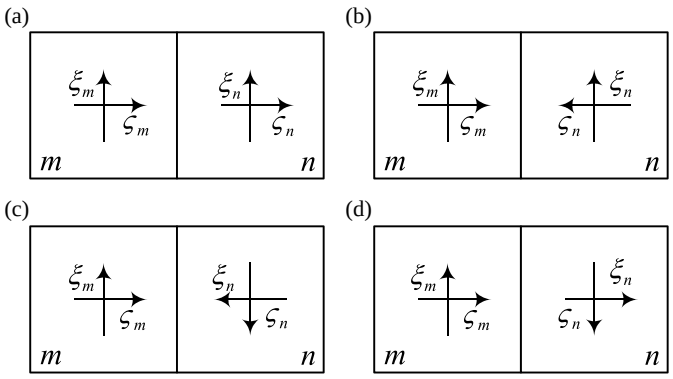

FIGURE 5. The possible local coordinate relationships between adjacent cells m and n.

of any mesh and calculate the impedance matrix correctly. The MoM based on hybrid domain basis functions can be applied to arbitrarily meshed local coordinates, thereby reducing the requirements on the geometric model to a minimum.

Based on the bilinear surface model, the hybrid domain basis function can be written as [36, 37]:

$$\vec{f}_{ij}^{u}(u,v) = \frac{(u^{i-1}+a_i u+b_i)v^{j-1}}{\left|\vec{e}_u \times \vec{e}_v\right|} \cdot \vec{e}_u \tag{32}$$

$$\vec{f}_{ij}^{v}(u,v) = \frac{(v^{j-1}+a_j v+b_j)u^{i-1}}{\left|\vec{e}_u \times \vec{e}_v\right|} \cdot \vec{e}_v \tag{33}$$

where $\vec{e}_u = d\vec{r}/du$, $\vec{e}_v = d\vec{r}/dv$.

Thus, based on this basis function, the target surface current is:

$$\begin{aligned}\vec{J}_s(u,v) &= \vec{J}_{su}(u,v) + \vec{J}_{sv}(u,v) \\ &= \sum_{i=1}^{M_u}\sum_{j=1}^{M_v-1} I_{ij}^{u}\vec{f}_{ij}^{u}(u,v) + \sum_{i=1}^{M_u-1}\sum_{j=1}^{M_v} I_{ij}^{v}\vec{f}_{ij}^{v}(u,v)\end{aligned} \tag{34}$$

M_u, M_v are the numbers of currents in the u, v directions on the bilinear quadrilateral cell, respectively, whose magnitude depends entirely on the size of the bilinear quadrilateral profile.

Thus, according to Galekin-MoM [38, 39], the integral equation of the objective can be written as the matrix equation:

$$[\mathbf{Z}_{kl}][\mathbf{I}_l] = [\mathbf{V}_k] \tag{35}$$

When filling the matrix equations, the matrix elements are arranged by combining the mutual coupling effects of the full-domain basis components and the partitioned basis components in the hybrid domain basis function.

4.4. Validation of Algorithm

To validate the effectiveness and accuracy of the PB-SM-MoM algorithm proposed in this paper, it is necessary to first verify the validity and correctness of the algorithm. During the verification process, the algorithm is used to calculate an instance of the composite scattering of a rough surface and a target, and the resulting calculation results are saved and plotted on a graph. The traditional MoM algorithm is used as the verification algorithm, which is mature and has high accuracy, although it is slow in calculation. However, it is a good choice for validation. Then, the traditional MoM method is used to calculate the same instance, and the calculation results are also plotted on the same graph. As shown in Fig. 6, it can be seen that the curves of the two algorithms are in good agreement, indicating that the PB-SM-MoM algorithm is effective in calculating the composite scattering of a rough surface and a target. For 20 calculations, the average time taken for PB-SM-MoM was 164 seconds, while the average time taken for MoM was 2498 seconds. Therefore, PB-SM-MoM was more than fifteen times faster than MoM. Programming in VC++ on a computer is with the following specifications: CPU frequency of 3.4 GHz and 8 GB of RAM.

The calculation instance is: Composite scattering model of a medium rough surface with a square conductor above, $f = 300$ MHz, the incident wave azimuth angle $\theta_i = 30°$; the size of the rough surface is $L_x \times L_y = 12\lambda \times 12\lambda$; the correlation length is $l_x \times l_y = 0.8\lambda \times 0.8\lambda$; the root mean square height is $h = 0.3\lambda$; the dielectric constant is $13.61 + 1.03i$; the side length of the cube is 1λ; and the height from the rough surface is 5λ.

In order to study the convergence of the algorithm in this paper with different composite models, the rough surface parameters are kept constant, and the upper conductor targets are replaced by cube, cylinder, and cuboid, respectively. The relationship between the number of iterations and the iteration error is calculated, and their variation curves are plotted in Fig. 7.

Figure 7(a) shows that under TE wave incidence, the error can be reduced to 10^{-6} after 14 iterations, while under TM wave incidence, the error can be reduced to 10^{-6} after 10 iterations, with good convergence and meeting the accuracy requirements. This convergence and accuracy requirement indicate that the algorithm proposed in this paper has excellent iterative convergence properties and can efficiently approach the optimal solution.

In addition, the advantage of this algorithm lies in its ability to adapt to different composite models and problem characteristics. Despite the differences in convergence speeds of different composite models, in general, as the number of iterations increases, the iterative errors decay exponentially, and the convergence effect is good and meets the accuracy requirements. This adaptability and convergence property make the algorithm have a wide range of application prospects, especially for large-scale problems and composite models, which can greatly improve computational efficiency and accuracy. It can be applied to various different composite models and problem scenarios.

5. CALCULATION RESULTS AND ANALYSIS

5.1. Effect of Target on Compound Scattering

This section uses the computational method proposed in this article to perform a detailed calculation of the composite scattering coefficients of a rough surface and its above cubic target, and the results are clearly plotted in Fig. 8. In order to more

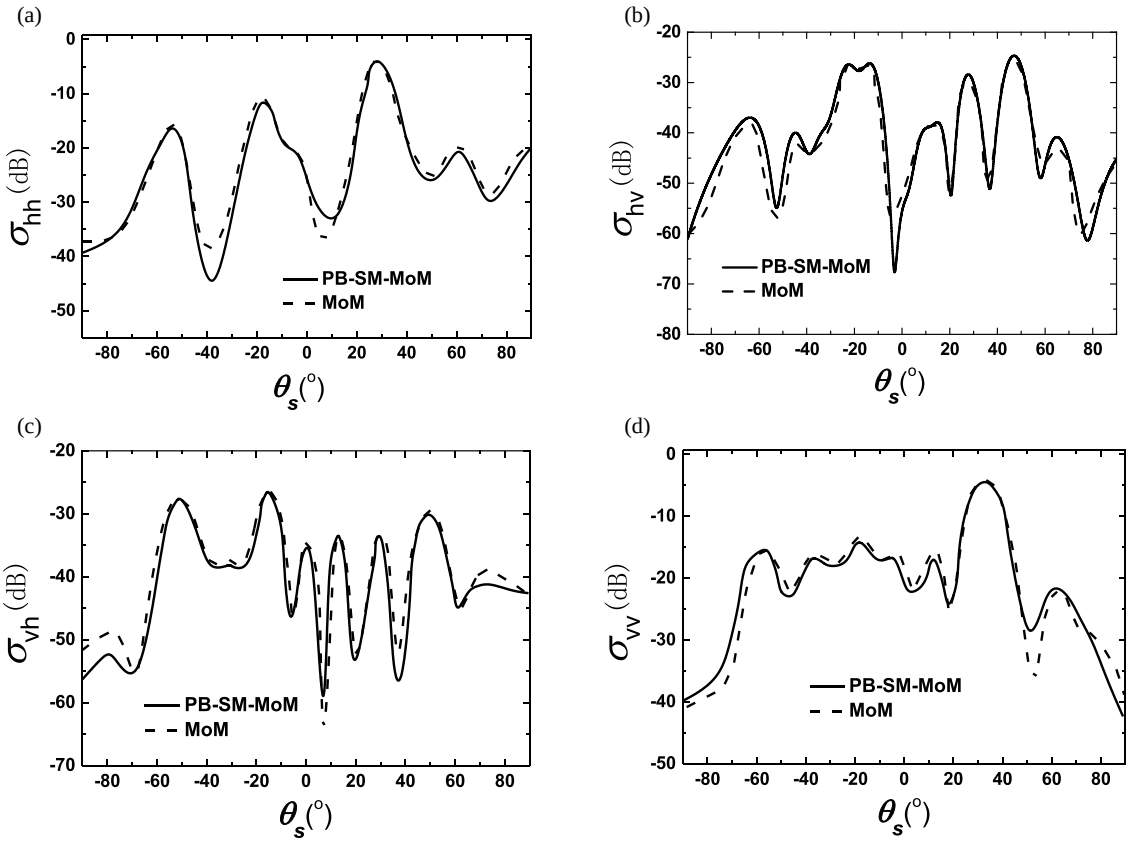

FIGURE 6. Validation of algorithm: (a) hh polarization, (b) hv polarization, (c) vh polarization, (d) vv polarization.

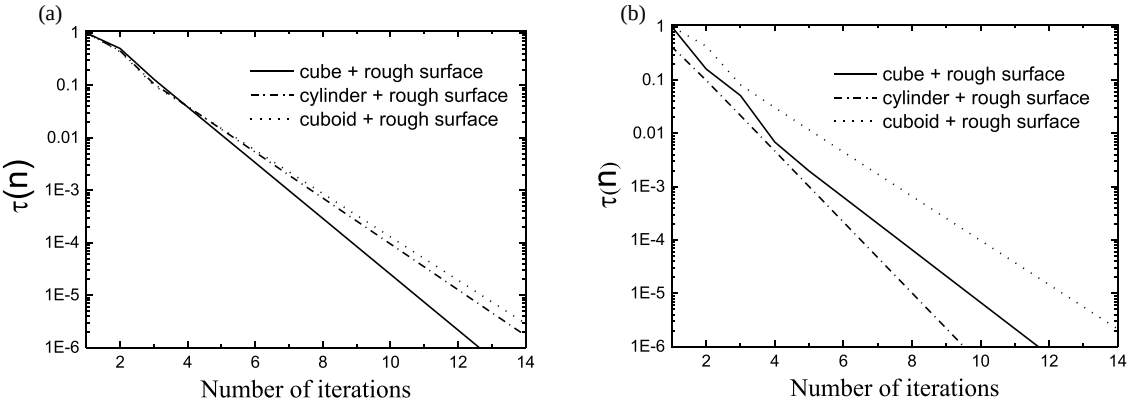

FIGURE 7. Error variation curve with the number of iterations: (a) TE incident wave and (b) TM incident wave.

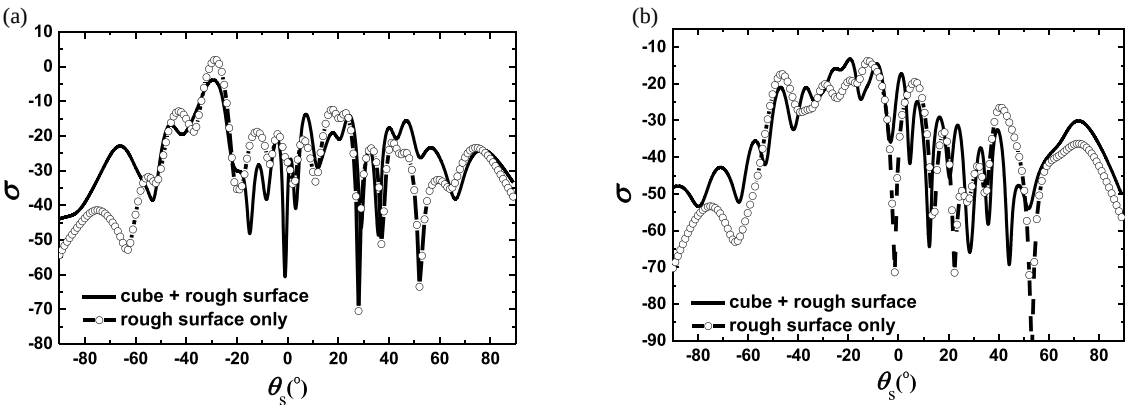

FIGURE 8. Effect of target on composite scattering: (a) TE incident wave and (b) TM incident wave.

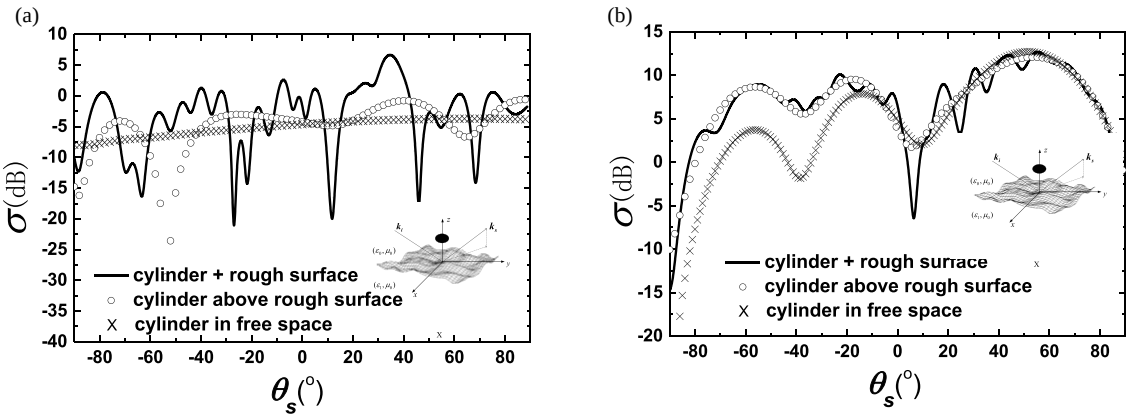

FIGURE 9. Effect of rough surface on composite scattering: (a) TE incident wave an (b) TM incident wave.

intuitively show the comparison effect, we also plot the scattering coefficient in Fig. 8 when only the rough surface exists. Observing the graph, it can be found that when there is a target above the rough surface, the scattering coefficient in all angular ranges except the specular direction increases significantly, especially in the backward scattering direction, with a more significant increase. In addition, it can also be concluded from the graph that the calculation result of TM wave is significantly lower than that of TE wave.

Observing Fig. 8, it can be found that when the target exists on the rough surface, its scattering coefficient is significantly larger than the scattering coefficient without the target. This difference reveals the interaction between the target and the rough surface. It is worth noting that under the TM wave incidence condition, the scattering coefficient of the target changes more significantly. This phenomenon has important theoretical guidance for target detection and recognition in the environmental background.

5.2. Effect of Rough Surface on Composite Scattering

Figure 9 shows the scattering results of only the cylinder, the composite scattering results of the cylinder interacting with the rough surface, and the total field model of the cylinder and rough surface without interaction (numerically equal to the direct sum of the scattering results of the cylinder and rough surface).

According to Fig. 9, we can further draw the following conclusions:

When only the cylinder exists without the rough surface, we can observe the weakest state of scattering. At this time, the change of scattering is relatively slow and slightly changes with the observation angle. However, this change is gradual, and the overall scattering intensity is very moderate.

However, when we consider the rough surface existing below the cylinder and there is a mutual coupling effect between the rough surface and the cylinder, the intensity of scattering is obviously enhanced, and the fluctuation of scattering becomes more significant. This fluctuation may mean that at some specific angles or frequencies, the scattering will be greatly enhanced or weakened, which provides more information for target detection and recognition.

Finally, when both the rough surface and target exist, the total field scattering intensity becomes strongest.

These findings have important practical significance for improving target detection and recognition technology. For example, by understanding the influence of background clutter on target RCS (radar cross-section), we can optimize the design and operation parameters of radar systems to better capture and recognize targets in complex background environments. In addition, these findings can also provide valuable information for fields such as military reconnaissance, remote sensing monitoring, and geophysical exploration to improve related detection and recognition technologies.

Further, the RCS of the aircraft target above the rough surface is investigated based on the algorithm in this paper, and the RCS of the pure aircraft target when there is no rough surface is given as a comparison. The results are plotted in Fig. 10.

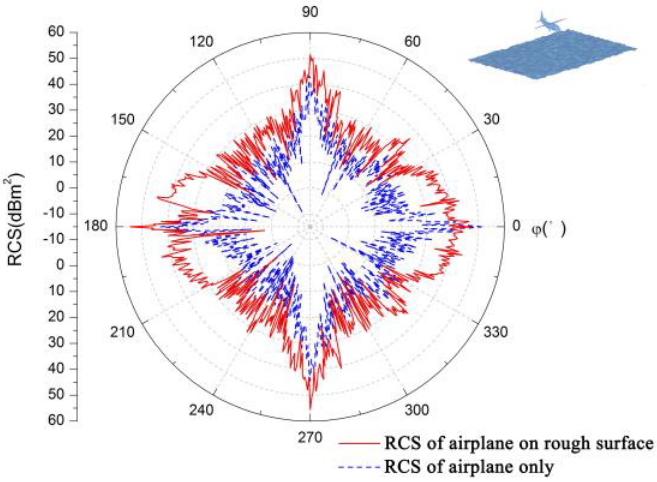

FIGURE 10. Environmental effect on target RCS.

The results obtained in this paper show that the coupling effect between the rough surface and the flying object significantly increases the rear RCS of the flying object on rough surfaces compared to the rear RCS without rough surface. Especially, in the direction of the flying object's head and tail, the

RCS of the flying object considering the rough surface effect is about 20 dB larger than that of the flying object without considering the rough surface effect, and there is no significant difference in the RCS on the two sides of the flying object. Therefore, using a reasonable appearance design can greatly inhibit the coupling scattering effect between the flying object and the environment, thus achieving the purpose of reducing the rear RCS of the flying object at certain angles (such as the direction of incoming cruise missiles), and greatly improving the survival ability of the flying object. The results obtained in this paper are consistent with the actual measurement results in the literature [40], which further validates the effectiveness of the algorithm used in this paper for calculating composite electromagnetic scattering characteristics. In addition, for the design of flying objects, more attention should be paid to the scattering effect on the head and tail of the flying object, in order to reduce the possibility of being detected and attacked by the enemy. At the same time, the scattering effect on the two sides of the flying object is relatively small, which can also be used as a reference for design. Through in-depth research on the influence of target roughness on electromagnetic scattering, it is expected to provide more accurate theoretical basis for related applications and further promote the development of electromagnetic scattering field.

6. CONCLUSION

In this paper, we have derived a coupled iterative integral equation system for rough surfaces and targets, and proposed a fast coupled iterative algorithm to calculate the complex three-dimensional scattering of conductive targets. In the model of complex electromagnetic scattering, there is mutual influence between the rough surface and the target, that is, the rough surface is not only irradiated by the incident wave but also irradiated by the scattering field of the target, and vice versa. Therefore, we combined the mutual influence of the rough surface and the target in the model of complex electromagnetic scattering, applied PB-SM to accelerate the scattering calculation of the rough surface, and applied the fast quadratic surface modeling of mixed-domain basis functions to quickly solve the target. Through iterative solution, we found that after 10 iterations, the error can be reduced to 10^{-6}, and the convergence rate can meet the actual calculation requirements.

Based on this algorithm, we conducted research and analysis on the composite scattering effect of targets and rough surfaces. The results show that through reasonable shape design, it is possible to reduce the RCS of the aircraft in certain angles (such as the direction of incoming cruise missiles) and improve the survivability of the aircraft. This research result has certain guiding significance for the design and optimization of conductive targets such as airplanes.

In future research, we will establish more algorithm models for different environments and targets, and consider researching coated targets to further enrich research results on composite electromagnetic scattering under different conditions. At the same time, we will also explore more efficient numerical calculation methods and optimization design strategies to improve calculation efficiency and design effect.

In conclusion, this paper provides an effective numerical calculation method and optimization design strategy for researching the complex electromagnetic scattering problem between rough surfaces and conductive targets. We believe that this research field will receive more extensive application and in-depth research in future development. Next, we will establish scattering models that match different environments and test them in both laboratory and practical applications.

REFERENCES

[1] Li, X., Y. Zhao, X. Liu, and Y. Cai, "Detection of a semi-rough target in turbulent atmosphere by an electromagnetic Gaussian schell-model beam," *Applied Sciences*, Vol. 9, No. 14, 2790, Jul. 2019.

[2] Ross, G., "Electromagnetic scattering and its applications," *Optica Acta: International Journal of Optics*, Vol. 29, No. 6, 725, 2010.

[3] Zitouni, A., L. Beheim, R. Huez, and F. Belloir, "Smart electromagnetic sensor for buried conductive targets identification," *IEEE Sensors Journal*, Vol. 6, No. 6, 1580–1591, Dec. 2006.

[4] Tantum, S. L. and L. M. Collins, "A comparison of algorithms for subsurface target detection and identification using time-domain electromagnetic induction data," *IEEE Transactions on Geoscience and Remote Sensing*, Vol. 39, No. 6, 1299–1306, Jun. 2001.

[5] Xi, H.-C., B. Li, W.-H. Mai, X. Xu, and Y. Wang, "Feature extraction for evaluating the complexity of electromagnetic environment based on adaptive multiscale morphological gradient and nonnegative matrix factorization," *Journal of Electrical and Computer Engineering*, Vol. 2022, Aug. 2022.

[6] Dong, J., "Hybrid electromagnetic signal feature extraction," *Wireless Communications and Mobile Computing*, Vol. 2022, 3693790, May 2022.

[7] Li, H., T. Xu, H. Lian, W. Chen, and D. Zhao, "Feature extraction and clustering of high dimensional electromagnetic interference signals based on multidimensional scaling and SOM network," in *Journal of Physics: Conference Series*, Vol. 2078, No. 1, 012072, 2021.

[8] Bian, Z., J. Li, and L. Guo, "Simulation and feature extraction of the dynamic electromagnetic scattering of a hypersonic vehicle covered with plasma sheath," *Remote Sensing*, Vol. 12, No. 17, 2740, Sep. 2020.

[9] Wu, Y., B. Ma, J. Shao, Y. Ji, and F. Teng, "Feature extraction and intelligent identification of induced polarization effects in 1D time-domain electromagnetic data based on PMI-FSVM algorithm," *IEEE Access*, Vol. 8, 150 478–150 488, 2020.

[10] Guo, X., Z. Wen, S. Li, and Q. Yang, "Study on the influence of blade on electromagnetic scattering characteristics in the open-ended cavity," *Journal of Computational Science*, Vol. 62, No. 6, 101716, Jul. 2022.

[11] Wang, Z. L., C. M. Tong, Y. J. Wang, Q. K. Wang, and G. X. Zou, "Study on environment modeling and electromagnetic scattering characteristics in mountainous areas," *Electromagnetics*, Vol. 42, No. 3, 192–209, Apr. 2022.

[12] Zheng, J., L. Hong, J. Gu, H. Duan, and Q. Zhang, "Research on wide-band electromagnetic scattering characteristics of random distributed objects using Monte Carlo method," *Journal of Computational Methods in Sciences and Engineering*, Vol. 21, No. 5, 1167–1177, 2021.

[13] Zou, G. X., C. Tong, H. L. Sun, and P. Peng, "Research on electromagnetic scattering characteristics of combined conducting

and dielectric target above coastal environment," *IEEE Access*, Vol. 8, 169 286–169 303, 2020.

[14] Bian, Z., J. Li, L. Guo, and X. Luo, "Analyzing the electromagnetic scattering characteristics of a hypersonic vehicle based on the inhomogeneity zonal medium model," *IEEE Transactions on Antennas and Propagation*, Vol. 69, No. 2, 971–982, Feb. 2021.

[15] Chen, Y., Z.-G. Hou, H.-C. Yin, and R.-S. Chen, "A novel PO solver for uncertainty EM computation of electrically large targets," *Applied Computational Electromagnetics Society Journal*, Vol. 35, No. 7, 750–757, Jul. 2020.

[16] Xiang, C., X. Dang, M. Li, F. Yang, and S. Xu, "Application of barycentric subdivision method for singularity integration in method of moments," *Applied Computational Electromagnetics Society Journal*, Vol. 35, No. 3, 250–257, Mar. 2020.

[17] Li, J., L. X. Guo, and H. Zeng, "FDTD investigation on electromagnetic scattering from two-dimensional layered rough surfaces," *Applied Computational Electromagnetics Society Journal*, Vol. 25, No. 5, 450–457, May 2010.

[18] Li, J., W. Meng, S. Chai, L. Guo, Y. Xi, S. Wen, and K. Li, "An accelerated hybrid method for electromagnetic scattering of a composite target-ground model and its spotlight SAR image," *Remote Sensing*, Vol. 14, No. 24, 6332, Dec. 2022.

[19] Wang, Q., C. Tong, X. Li, Y. Wang, Z. Wang, and T. Wang, "Composite electromagnetic scattering and high-resolution SAR imaging of multiple targets above rough surface," *Remote Sensing*, Vol. 14, No. 12, 2910, Jun. 2022.

[20] Liu, J., H. Chen, H. Zhang, J. Yuan, and Z. Li, "A modified hybrid integral equation to electromagnetic scattering from composite PEC-dielectric objects containing closed-open PEC junctions," *Applied Computational Electromagnetics Society Journal*, Vol. 36, No. 6, 642–649, 2021.

[21] Huang, Y., Z. Zhao, X. Li, Z. Nie, and Q.-H. Liu, "Volume equivalent SBR method for electromagnetic scattering of dielectric and composite objects," *IEEE Transactions on Antennas and Propagation*, Vol. 69, No. 5, 2842–2852, May 2021.

[22] Ma, C., Y. Wen, and J. Zhang, "A fast, hybrid, time-domain discontinuous Galerkin-physical optics method for composite electromagnetic scattering analysis," *Applied Sciences*, Vol. 11, No. 6, 2694, Mar. 2021.

[23] Tian, W., B. Wei, and X.-B. He, "A novel domain decomposition-finite difference time domain method for composite scattering from a target above rough surface," *Waves in Random and Complex Media*, Vol. 31, No. 2, 255–269, Mar. 2021.

[24] Wang, K. C., J. Liu, J. H. Xu, X. T. Fan, and L. R. Zhang, "An adaptive nested complex source beam method for electromagnetic scattering of composite conducting-dielectric objects," *Engineering Analysis with Boundary Elements*, Vol. 118, 244–249, Sep. 2020.

[25] He, W.-J., X.-W. Huang, M.-L. Yang, and X.-Q. Sheng, "Massively parallel multilevel fast multipole algorithm for extremely large-scale electromagnetic simulations: A review," *Progress In Electromagnetics Research*, Vol. 173, 37–52, 2022.

[26] Zhan, Q., Y. Fang, M. Zhuang, M. Yuan, and Q. H. Liu, "Stabilized DG-PSTD method with nonconformal meshes for electromagnetic waves," *IEEE Transactions on Antennas and Propagation*, Vol. 68, No. 6, 4714–4726, Jun. 2020.

[27] Ye, H. and Y.-Q. Jin, "A hybrid KA-MoM algorithm for computation of scattering from a 3-D PEC target above a dielectric rough surface," *Radio Science*, Vol. 43, No. 3, 2008.

[28] Chai, S.-R., F.-Y. Zhu, J. Li, Z.-X. He, Y.-F. Zou, Y.-W. Wei, K. Li, L.-X. Guo, and L. Li, "Electromagnetic scattering and Doppler spectrum simulation of land-sea junction composite rough surface," *Remote Sensing*, Vol. 15, No. 3, 836, Feb. 2023.

[29] Guo, G., L. Guo, R. Wang, W. Liu, and L. Li, "Transient scattering echo simulation and ISAR imaging for a composite target-ocean scene based on the TDSBR method," *Remote Sensing*, Vol. 14, No. 5, 1183, Mar. 2022.

[30] Liang, Y. and L. X. Guo, "A study of composite scattering characteristics of movable/rotatable targets and a rough sea surface using an efficient numerical algorithm," *IEEE Transactions on Antennas and Propagation*, Vol. 69, No. 7, 4011–4019, Jul. 2021.

[31] He, H.-J. and Y. Zhang, "An effective method for electromagnetic scattering from a coated object partially buried in a dielectric rough surface," *Journal of Electromagnetic Waves and Applications*, Vol. 35, No. 6, 754–765, Apr. 2021.

[32] Pan, G. W., *Wavelets in Electromagnetics and Device Modeling*, John Wiley & Sons, 2003.

[33] Yu, X. N., "Simulation of random rough surface based on Monte Carlo method," *Value Engineering*, Vol. 36, No. 8, 226–228, 2017.

[34] Ji, W.-J. and C.-M. Tong, "Bistatic scattering from three-dimensional target on perfectly conducting rough surface by using G-SMFSIA/CAG," *Acta Physica Sinica*, Vol. 60, No. 1, 010301, Jan. 2011.

[35] Tsang, L., J. A. Kong, K.-H. Ding, and C. O. Ao, *Scattering of Electromagnetic Waves: Numerical Simulations*, John Wiley & Sons, New York, 2001.

[36] Popović, B. D. and B. M. Kolundžija, *Analysis of Metallic Antennas and Scatterers*, The Institution of Electrical Engineers, London, 1994.

[37] Djordjevic, M. and B. M. Notaros, "Double higher order method of moments for surface integral equation modeling of metallic and dielectric antennas and scatterers," *IEEE Transactions on Antennas and Propagation*, Vol. 52, No. 8, 2118–2129, 2004.

[38] Reddy, C. J., M. D. Deshpande, C. R. Cockrell, and F. B. Beck, "Fast RCS computation over a frequency band using method of moments in conjunction with asymptotic waveform evaluation technique," *IEEE Transactions on Antennas and Propagation*, Vol. 46, No. 8, 1229–1233, 1998.

[39] Donepudi, K. C., K. Gang, J. M. Song, and W. C. Chew, "Higher-order MoM implementation to solve integral equations," in *IEEE International Symposium on Antennas and Propagation Society*, Vol. 3, 1716–1719, 1999.

[40] Jia, G., P. Yin, S. Shao, and J. Wang, "Review of RCS measurement and imaging methods of stealth aircraft," *Journal of National University of Defense Technology*, Vol. 44, No. 3, 93–103, 2022.